Interband spin–orbit coupling between anti-parallel spin states in Pb quantum well states

Bartosz Slomski[1,2]**, Gabriel Landolt**[1,2]**, Stefan Muff**[1,2]**,
Fabian Meier**[1,2]**, Jürg Osterwalder**[1] **and J Hugo Dil**[1,2,3]

[1] Physik-Institut, Universität Zürich, Winterthurerstrasse 190, CH-8057 Zürich, Switzerland
[2] Swiss Light Source, Paul Scherrer Institut, CH-5232 Villigen, Switzerland
E-mail: jan-hugo.dil@psi.ch

Abstract. Using spin and angle-resolved photoemission spectroscopy we investigate a momentum region in Pb quantum well states on Si(111) where hybridization between Rashba-split bands alters the band structure significantly. Starting from the Rashba regime where the dispersion of the quasi-free two-dimensional electron gas is well described by two spin-polarized parabolas, we find a breakdown of the Rashba behavior which manifests itself (i) in a spin splitting that is no longer proportional to the in-plane momentum and (ii) in a reversal of the sign of the momentum splitting. Our experimental findings are well explained by including interband spin–orbit coupling that mixes Rashba-split states with *anti-parallel* rather than parallel spins. Similar results for Pb/Cu(111) reveal that the proposed hybridization scenario is independent on the supporting substrate.

[3] Author to whom any correspondence should be addressed.

IOP Institute of Physics ⏀ DEUTSCHE PHYSIKALISCHE GESELLSCHAFT

Contents

1. Introduction

The study of the spin structure of non-magnetic low dimensional systems by means of spin- and angle-resolved photoelectron spectroscopy (SARPES) has intensified in recent years [1]. One of the driving forces has been the discovery of systems with a large Rashba-type spin splitting on a variety of three-dimensional [2, 3], two-dimensional [4–6] and even one-dimensional systems [7–9]. The fact that for topological insulators the topology of the bulk bands is reflected in the spin structure of the surface states [10] provided a further boost to this type of experiments. Also here a variety of SARPES experiments have been performed in order to elucidate the details of the spin-structure and the variations from a purely in-plane helical spin system [11–15]. In most of these cases the initial state has been considered as a pure spin state although under the influence of strong spin–orbit interaction the spin is no longer a good quantum number. Recently it has been shown that due to the orbital mixing in the topological surface state of Bi_2Se_3 also the spin structure of this state consists of mixed spin states [16].

Also for Rashba systems deviations from the pure spin scenario are expected to occur when spin–orbit coupling (SOC) induced avoided crossing hybridization leads to an opening of energy gaps between Rashba-split bands. When bands belonging to the same group representation approach one another, SOC opens a hybridization gap, resulting in an avoided crossing of bands that is absent within a nonrelativistic treatment. Close to the gap the Bloch eigenstates get mixed and form new eigenstates. Since the driving mechanism for the mixing of the states is SOC whose operator ($\xi \mathbf{L} \cdot \mathbf{S}$) contains both a spin-conserving and a spin-flip term [17], we would like to understand how the SOC-induced hybridization alters the properties of an initially Rashba-split two-dimensional electron gas (2DEG).

To date, only few experiments have investigated the subtle interplay between the orbital momentum and spin of hybridized states using the direct method of SARPES. For example Rybkin *et al* [18] found that quantum well states (QWS) in the low-Z material aluminum deposited on the high-Z substrate W(110) acquire large spin splittings through the interaction with spin-polarized interface states because of the avoided crossing hybridization. In Ag films grown on Si(111) and covered with the $\sqrt{3}$-Bi–Ag alloy, it has been shown that spin-selective hybridization occurs between spin-degenerate Ag QWS and strongly Rashba-type spin-split alloy surface states [19, 20]. In both studies the authors observed a hybridization between states with parallel spin direction. In contrast to this, first-principles calculations and ARPES measurements of Bi/Cu(111) [21] and $BiAg_2$ [22] indicate a hybridization between states with

anti-parallel spin direction. Whether the former (hybridization between parallel spins) or the latter (hybridization of *anti-parallel* spins) scenario is present in a system depends on the orbital symmetry of the involved wave functions.

As a model system we investigate QWS in an ultra-thin Pb film grown on the Bi reconstructed Si(111) substrate. The studied energy-momentum region contains a single and pronounced electron-like band spin-split by the Rashba effect which starts to deviate from the parabolic dispersion at larger wave vectors. The electronic and structural properties of Pb QWS on Si(111) have been intensively studied in the past. The reason for the large interest is because Pb on Si(111) shows a rich variety of phenomena ranging from anomalies in the superconducting transition temperature [23–25], the formation of magic height islands [26], extremely long excited-state lifetimes [27], structure dependent Schottky barriers [28, 29], interface dependent effective mass [30] and Rashba-type spin splitting [31, 32]. Here we add the new phenomenon of interband SOC between Rashba-type spin-split QWS of opposite spin directions.

By means of SARPES combined with a vectorial spin analysis [33] we identify an interband SOC caused by the spin-flip term of the SOC operator. Our findings are well matched by a simple analytical model adapted from [22]. Similar behavior is observed experimentally in Pb QWS grown on Cu(111).

2. Experiment

The (S)ARPES experiments were performed with the COPHEE setup at the Surface and Interface Beamline at the Swiss Light Source of the Paul–Scherrer–Institut [34]. The energy and angular resolution of the spectrometer in the spin-integrated (spin-resolved) ARPES measurements were set to 30 (80) meV and 0.5° (1.5°), respectively. All valence band photoemission data were recorded at a photon energy of 24 eV due to the optimal photoemission cross-section [35], with p-polarized light. The base pressure of the chamber was below 2×10^{-10} mbar and the sample temperature during the measurements was $T < 80$ K. The n-type Si(111) (44–62 Ω cm) sample was degassed at 600 K for 24 h and flashed several times above 1300 K to remove adsorbates and to form the (7×7) surface reconstruction [36]. The cleanliness of the sample was checked with ARPES, where the surface states could be identified, and by inspecting the low-energy electron diffraction (LEED) pattern which showed the typical (7×7) surface reconstruction with intense superstructure spots. The Bi interface with $(\sqrt{3} \times \sqrt{3})R30°$ symmetry and 1 monolayer (ML) coverage in substrate units (1 ML = 7.83×10^{14} atoms cm^{-2}) (henceforth Bi-$\sqrt{3}$) was prepared through the deposition of approximately 3 ML of Bi from a water-cooled Knudsen cell onto the clean Si(111)-(7×7) surface at low temperature and subsequent annealing until the $(\sqrt{3} \times \sqrt{3})R30°$ surface reconstruction appeared in LEED [37]. On this reconstructed substrate a thin crystalline Pb film was grown by depositing at a rate of $\frac{1}{3}$ ML per minute after cooling down again to below 100 K. Under these conditions Pb grows in a layer-by-layer mode allowing for a precise determination of the layer thickness through monitoring the binding energies of the subbands as a function of deposition time. The ultra-thin Pb film on Cu(111) was fabricated by the deposition of Pb from a water-cooled e-beam evaporator, at a pressure below 3×10^{-10} mbar, onto a Cu(111) sample held at 80 K. The single crystal Cu(111) was cleaned before deposition by several cycles of Ar ion bombardment and annealing.

3. The Rashba–Bychkov effect

The Rashba model was originally proposed to describe the motion of an electron in a 2DEG subjected to the electric field due to a broken structural inversion symmetry perpendicular to the plane of confinement, i.e. $\mathbf{E} = E\mathbf{e_z}$. In such an environment the electric field acts as a magnetic field in the rest frame of a moving electron with momentum $\hbar\mathbf{k}_\parallel$ as represented by the Rashba Hamiltonian

$$\hat{H}_{RB} = \alpha_{RB}(\mathbf{e_z} \times \mathbf{k}_\parallel) \cdot \mathbf{S}. \tag{1}$$

Here $\alpha_{RB} \propto E_z$ is the so-called Rashba parameter which describes the strength of the interaction between the spin $\mathbf{S}$ of an electron and the effective magnetic field $\mathbf{B_{eff}} \propto (\mathbf{e_z} \times \mathbf{k}_\parallel)$. The Rashba effect is therefore in close analogy to the Zeeman effect, except that the quantization axis for the spin, defined by $\mathbf{B_{eff}}$, is a function of both, the momentum of the electron and the electric field. Owing to the Rashba effect the initially two-fold degenerate parabolic dispersion splits into two parabolas with oppositely spin-polarized states:

$$E^{\pm}(\mathbf{k}_\parallel) = E_{\bar{\Gamma}} + \frac{\hbar^2}{2m^\star}\mathbf{k}_\parallel^2 \pm \alpha_{RB}|\mathbf{k}_\parallel|, \tag{2}$$

where $E_{\bar{\Gamma}}$ is the binding energy at $k_\parallel = 0\,\text{Å}^{-1}$ and $m^\star$ represents the effective mass of the electrons.

The Rashba effect has been experimentally confirmed in many systems, such as in semiconductor heterostructures [38], in Shockley-type surface states on noble metals, e.g. Au(111) [39–41] and recently in Cu(111) [42], in surface states of heavy metal surface alloys [4, 43–46], on semiconducting surfaces covered with heavy metals [5, 47], and in one monolayer of Bi on Cu(111) [48]. Many insights into the origin and the strength of spin–orbit interaction have been achieved by studying these systems [49]. Nowadays it is accepted that the size of the Rashba effect in real systems is not a simple function of the electric field at the surface or interface, but that it is more sensitive to the details of the wave function close to the nuclei which in turn are related to structural properties of the surface.

A nice playground for this model is the Rashba effect in Pb QWS [31, 32]. Figure 1(a) shows the in-plane electronic structure of an ultra-thin film formed by 10 ML of Pb grown on the Bi reconstructed Si substrate and measured with ARPES. The M-shaped QWS with a binding energy (E_b) $E_{b,\bar{\Gamma}} = 490\,\text{meV}$ at normal emission ($k_\parallel = 0\,\text{Å}^{-1}$) arises from the quantization of the band dispersion along the Γ–L direction due to the size reduction which is illustrated in the left panel of figure 1(b) by the example of a 8 ML Pb film. The corresponding in-plane band structure of the ultra-thin Pb film is shown in the right panel of figure 1(b) and was calculated with density functional theory using the *Wien2k* simulation package [50] incorporating SOC.

Our previous research focused on the spin texture of the bands in the momentum region around the surface Brillouin zone (SBZ) center. Here the system is a good approximation of a quasi-free 2DEG confined in a quantum well with a structural inversion asymmetry. We could show that these states show a Rashba effect and that the size of the spin splitting is sensitive to the metal–substrate interface. In the first approach we have varied the chemistry of the interface by studying various interfactants such as Pb, Bi and Ag, which form highly regular structures of $\sqrt{3}$ symmetry on Si(111). It is found that the size of the Rashba effect changes dramatically between these interfaces: replacing the Pb interface by a Bi layer reduced the Rashba parameter by 60%, whereas QWS in Pb films grown on a Ag reconstructed Si
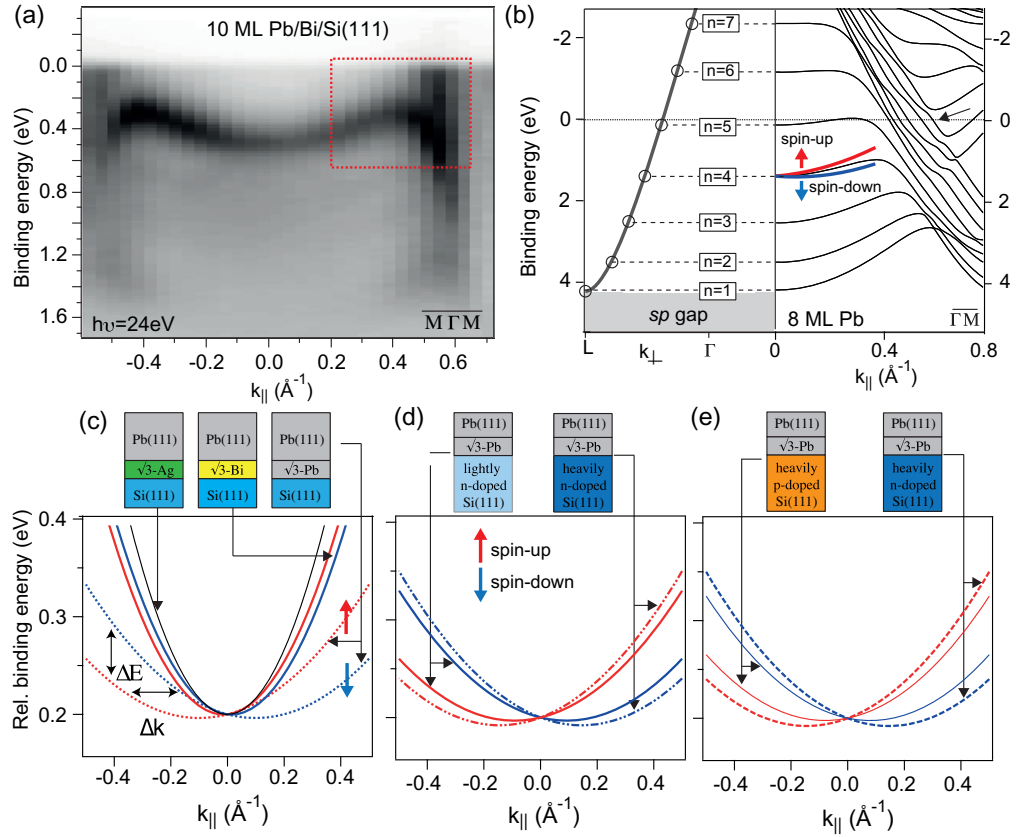
Figure 1. (a) Electronic structure of 10 ML Pb on Bi- $\sqrt{3}$/Si(111) measured with angle-resolved photoemission spectroscopy. (b) Quantization of the band structure along $k_\perp$ as a consequence of size reduction along the growth direction (left panel). Calculated band structure of a 8 ML free-standing Pb film (right panel). The subband with the quantum number $n = 4$ is schematically spin-split into two spin-polarized parabolas with opposite spin direction according to the Rashba effect. (c)–(e) Spin-split parabolas obtained using parameters (α_{RB} and $m^\star$) as deduced from the (S)ARPES experiment to illustrate the sensitivity of the Rashba effect on (c) the interface chemistry, (d) the donor concentration and (e) the type of dopant. Note that the band dispersions are displayed on a relative binding energy scale to illustrate also the differences in the effective mass as a function of interface.

substrate showed no measurable spin splitting [32], see figure 1(c). The sensitivity of the Rashba parameter to the donor concentration of the Si substrate revealed a very promising pathway toward the realization of a spintronic device: by increasing the donor concentration by a factor of 20, we could tune the Rashba parameter by a factor of two [51], see figure 1(d). A strong sensitivity of the Rashba parameter is also found when changing the type of dopant, while keeping the dopant concentration almost constant (figure 1(e)). These changes of the Rashba effect are well understood by a modified charge density distribution within the Pb film as a consequence of an interface and doping dependent Schottky barrier [51].
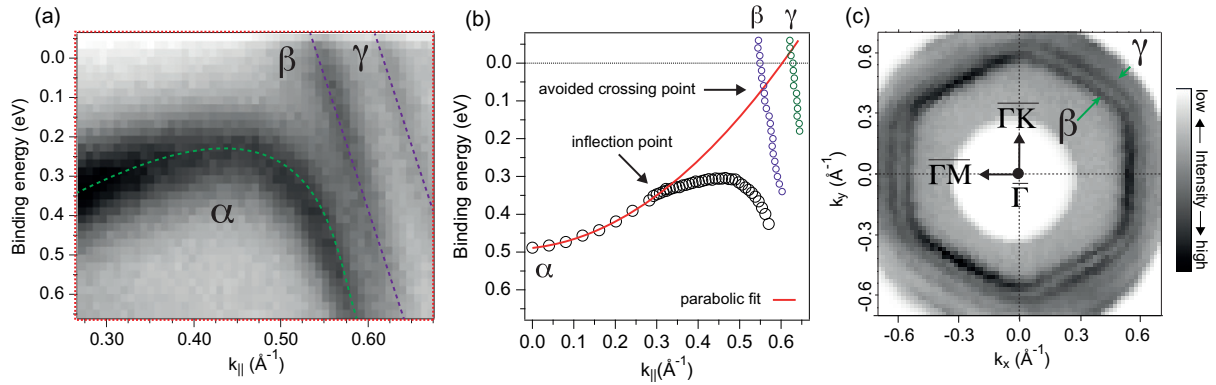
Figure 2. (a) Band structure region where the SOC-induced avoided crossing hybridization leads to the pronounced deviation from the parabolic dispersion of the α-band. (b) Extracted dispersion of the α, β and γ band. The parabolic fit gives an effective mass of $m^\star = 3.2 m_e$ and starts to deviate from the actual dispersion at $\approx 0.3\,\text{Å}^{-1}$. (c) Fermi surface of the ultra-thin Pb film (10 ML) with the high-symmetry direction $\overline{\Gamma} - \overline{M} \parallel k_x$ and $\overline{\Gamma} - \overline{K} \parallel k_y$.

4. Interband spin–orbit coupling in Pb quantum well states

The main focus of the present study is the outer region in the band structure marked by the dashed box in figure 1(a) and enlarged in figure 2(a). It consists of three bands labeled as α, β, γ, which are derived from Pb 6p orbitals because the binding energies lie above the Pb sp symmetry band gap in the Γ–L direction (cf figure 1(b)) [52]. More specifically, states that are described by an upward parabolic dispersion with band minimum at $\overline{\Gamma}$ are mainly of $6p_z$ symmetry (magnetic quantum number $m_l = 0$), whereas states with downward dispersion and an unoccupied band maximum at $\overline{\Gamma}$ are of $6p_{x,y}$ symmetry ($m_l \pm 1$). Within a momentum range of $k_\parallel = \overline{\Gamma} \pm 0.3\,\text{Å}^{-1}$, the dispersion of the α-band is well described as a Rashba system via equation (2) with an effective mass of $m^\star = 3.2 m_e$ [30] and a Rashba parameter of $\alpha_{RB} = 0.033\,\text{eV}\,\text{Å}$ [32]. Remarkably, the initially $6p_z$ derived α-band changes its curvature from being electron-like ($m^\star > 0$) to hole-like ($m^\star < 0$) for in-plane momenta $|k_\parallel\rangle 0.3\,\text{Å}^{-1}$, which is a first indication of hybridization [53]. Such a pronounced change in the electronic dispersion has been also observed for monolayers of Pb on graphitized SiC and explained as due to SOC-induced hybridization and is therefore related to the peculiar band structure of the Pb film [54]. In figure 2(b) we plot the dispersion of the α-band, which was obtained by fitting energy distribution curves utilizing Voigt profiles, as a function of momentum. It is seen that the actual electron-like dispersion starts to deviate from the experimental data at $k_\parallel \approx 0.32\,\text{Å}^{-1}$ (hereafter termed the inflection point). For clarity we have also included the dispersions of the hole-like β and γ bands, respectively. The parabolic fit of the α-band would intersect the β-band at $(E_b, k_\parallel) \approx (100\,\text{meV}, 0.55\,\text{Å}^{-1})$ (hereafter termed the avoided crossing point) in case the SOC-induced hybridization were turned off. The Fermi level crossing of the β- and γ-band is also nicely resolved in figure 2(c) which displays the Fermi surface (FS) of the ultra-thin Pb film. The hexagonal shape of the FS reflects the (111) crystal symmetry with corners pointing into the high symmetry direction $\overline{\Gamma} - \overline{K}$. Furthermore, by following e.g. the inner $6p_{x,y}$ band on the FS we observe an intensity modulation with a periodicity of $\frac{2}{3}\pi$, in line with the three-fold rotational symmetry (C_{3v}) of the crystal structure.

Motivated by the peculiar dispersion of the α-band we first study the evolution of its spin splitting as a function of momentum, starting in the Rashba regime. In figure 3(a) we show spectra recorded as a function of $k_\parallel$ extracted from figure 2(a). We start with a spin-resolved energy distribution curve (SR-EDC) taken at $k_\parallel = 0.29\,\text{Å}^{-1}$ using the two-Mott detector scheme, which is sensitive to all three spin polarization components (P_x, P_y, P_z) [34] which are defined as the expectation value of the spin operator, i.e. $P_i = \langle \Psi | S_i | \Psi \rangle$ with $i = x, y, z$.

At this particular momentum, far away from the region where the α-band bends downward, we expect a Rashba-like spin splitting and spin orientation. The data and the corresponding results using the self-consistent vectorial spin analysis [44] are shown in figure 3(b). We observe up–down excursions in the tangential spin polarization (P_{tan}), the direction perpendicular to the momentum, and a spin splitting of $\Delta E = 20\,\text{meV}$ ($\Delta E := E_b^\downarrow - E_b^\uparrow$) between the spin-up and spin-down states. The polarization along the radial direction is below the detection limit of the spectrometer. An out-of-plane spin polarization (P_z), which has been reported for this system [32], is suppressed because we measured along the $\overline{\Gamma}$–$\overline{M}$ direction, i.e. in a mirror plane of the (1×1) SBZ.

In the following we switch to the single Mott scheme and focus on the tangential spin polarization component. This way, we can decrease the Δk steps for similar overall acquisition time and precisely follow the evolution of the spin splitting along the dispersion. Figure 3(c) shows exemplary P_{tan} data and fits obtained from SR-EDCs taken at increasing in-plane momenta. The color coding of the data corresponds to that in figure 3(a). We observe first an increased polarization amplitude and spin splitting toward $k_\parallel = 0.34\,\text{Å}^{-1}$, followed by a reduction toward $k_\parallel = 0.5\,\text{Å}^{-1}$ (see also figure 5(a)).

In the region where the α-band bends downward the spin splitting seems to recover again with the same sign of the spin splitting, i.e. $\Delta E = 2\alpha_{\text{RB}} k_\parallel > 0$, which indicates a sign reversal in the momentum splitting Δk. As will be shown later, this sign change is better resolved in spin-resolved momentum distribution curves (MDC) rather than SR-EDCs. At this point we notice that in the region beyond the inflection point the tangential spin alignment persists and neither radial nor out-of-plane rotations of the spin polarization vector are observed. This is exemplified in figure 3(d) which shows the 3D spin polarization data measured at $k_\parallel = 0.36\,\text{Å}^{-1}$. The spin polarization vectors of the two Rashba-split states are very similar to those displayed in figure 3(b).

Next, we focus on the spin texture of the α- and the β-band by analyzing SR-MDCs. Figure 4(a) shows spin-integrated MDCs extracted from figure 2(a). Starting from the high binding energy side, we observe maximum spectral weight on the downward dispersing α-band and a small shoulder at the high momentum tail from the β-band. With decreasing E_b the spectral weight shifts from the α- to the β-band. Closer to E_F both the β and γ bands can be clearly distinguished. Figure 4(b) shows a series of spin polarization data from SR-MDCs. The polarization curve at $E_b \approx 0.6\,\text{eV}$ (scan 7) reveals a momentum splitting of the α-band, that is in line with data taken in the EDC mode (cf figures 3(c) and (b)), i.e. $k_{\alpha,\parallel}^\downarrow < k_{\alpha,\parallel}^\uparrow$ translates into $\Delta E > 0$. This substantiates our finding that the sign of the momentum splitting of the α-band reverses upon passing the avoided crossing point. Because for this band both the sign of $m^\star$ and the sign of Δk changes, a locally defined Rashba parameter would maintain its sign since $\alpha_{\text{RB}} = \hbar^2 \Delta k / 2m^\star$. This is similar to calculations for W(110) and Al/W(110) [55].

However, for the adjacent β-band we find a sign reversal of the Rashba parameter. This is seen from a comparison between the measurements at $E_b \approx 0.6\,\text{eV}$ and E_F (figure 4(b)). Scan 7 indicates that the spin-up peak (indicated by the second up-arrow at $k_\parallel \approx 0.64\,\text{Å}^{-1}$) is located
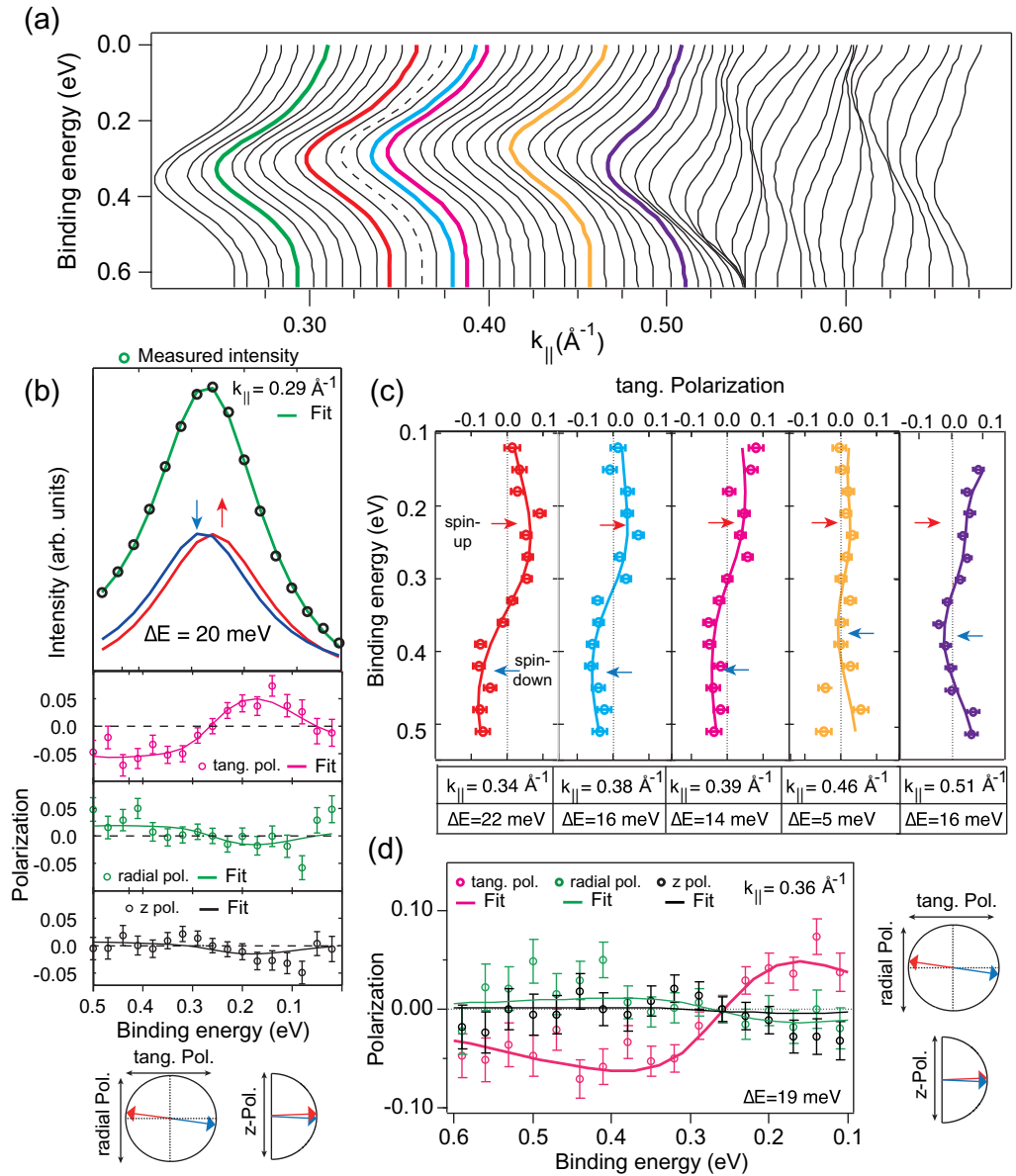
Figure 3. (a) Energy distribution curves of the α-band as a function of $k_\parallel$. (b) (upper panel) Measured spin-integrated EDC at $k_\parallel = 0.29\,\text{Å}^{-1}$ with Voigt intensity profiles obtained from the two-step fitting routine. (middle panel) Corresponding spin polarization data and fits in the tangential, radial and z-direction. (lower panel) Spin polarization vectors revealed from the fit. (c) Tangential polarization data and fits at increasing in-plane momenta toward the avoided crossing point. (d) Measured spin polarization data and fits (left panel) and polarization vectors (right panel) in the hybridization regime ($k_\parallel = 0.36\,\text{Å}^{-1}$).

at lower $k_\parallel$ than the corresponding spin-down peak (not measured). In contrast, the analysis of scan 1 reveals that the spin-down peak of the β-band is at lower momentum ($k_\parallel \approx 0.53\,\text{Å}^{-1}$) than the corresponding spin-up peak ($k_\parallel \approx 0.59\,\text{Å}^{-1}$). This means, in between $E_\text{b} = 0.6\,\text{eV}$ and E_F
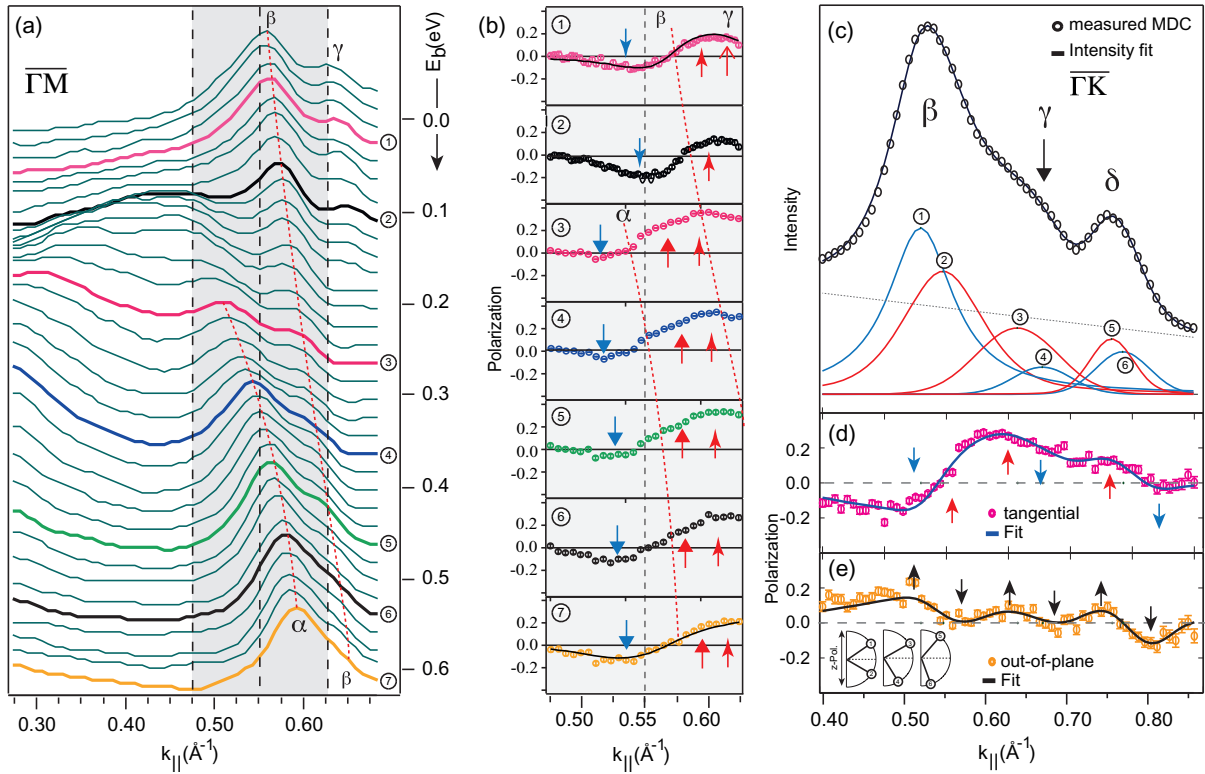
Figure 4. (a) Spin-integrated MDC along $\overline{\Gamma}$– $\overline{M}$ as a function of binding energy. (b) Measured tangential spin polarization data at various values of E_b; the numbers correspond to those in (a). (c) Measured total intensity MDC at the Fermi level along $\overline{\Gamma}$– $\overline{K}$ and corresponding spin polarization data and fits along the tangential direction (d) and the z-direction (e). The inset of (e) shows the out-of-plane rotation of the spin polarization vectors at increasing in-plane momentum obtained from the self-consistent two-step fit.

the Rashba parameter of the band changed its sign as it disperses toward E_F. Indeed, when we compare scan 3 (at $\approx 0.25\,\text{eV}$) with scan 2 (at $\approx 0.1\,\text{eV}$) we can localize this sign change, which is close to the avoided crossing point (cf figure 2(b)). The behavior is therefore different from the one of the α-band, where both the sign of the effective mass and the sign of the momentum splitting are changed.

To unravel how the spin textures of these bands interplay, we have performed a SR-MDC (single Mott) at the Fermi level in an extended momentum range and along the $\overline{\Gamma}$– $\overline{K}$ high symmetry direction. The results are shown in figures 4(c)–(e). First of all, the larger measured momentum range allows to investigate the spin texture of three $p_{x,y}$ bands (β, γ, δ) at the Fermi level. Figure 4(c) shows the spin-integrated MDC, and in (d) and (e) we show tangential and out-of-plane polarization data together with our analysis, respectively. There is a clear difference between the P_z and P_{tan} data. While the z-polarization reveals a spin configuration of alternating up–down spin pairs, the tangential polarization shows down–up–up–down–up–down excursions. This means that the Rashba parameter changes sign between the β-band and the γ-band. Furthermore, it is found that the out-of-plane rotation of the spin polarization vector increases with the in-plane momentum, which is understood by the fact that states of mainly
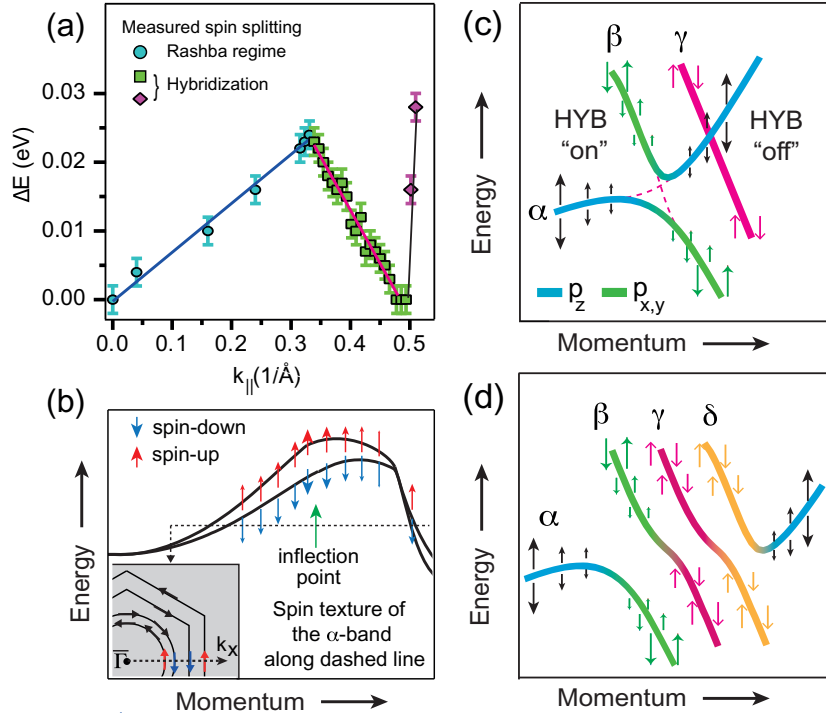
Figure 5. (a) Measured k-dependent energy splittings of the α-band over the full investigated momentum range, and linear fits. (b) Schematic drawing of the band splitting deduced from our fitting procedure to the experimental data. The inset shows the spin texture along the dashed line across the constant energy surface, illustrating the sign reversal of the momentum splitting. (c) Schematic drawing of the resulting dispersion of the α- and the β-band when SOC-induced hybridization is taken into account. When the hybridization is locally turned off, the β-band continues with an electron-like dispersion and crosses the γ-band. (d) Resulting schematic dispersion of the bands after hybridization is turned on between the α- and the β-band, between the β- and the γ-band, and between the γ- and the δ-band.

$p_{x,y}$ orbital symmetry are more sensitive to the in-plane gradient of the potential. This finding is nicely in line with the observations for the high-Z metal surface alloys, e.g. Bi/Ag(111) [44].

We start the discussion on the origin of the measured spin structure with the right panel of figure 1(b) which displays a band structure calculation of a free-standing 8 ML Pb film. The avoided crossings of the bands are well reproduced by taking SOC into account as already demonstrated in [54]. At larger momenta it is seen that the $p_{x,y}$ band that crosses E_F at $k_\parallel \approx 0.6\,\text{Å}^{-1}$ (the crossing is marked by an arrow), continues with an electron-like dispersion, adapted from an electron-like band (originally the α-band), as long as no hybridization with a neighboring $p_{x,y}$ band occurs. As will be shown below this property has an important influence on the spin texture of the downward dispersing bands in between.

Figures 5(a) and (b) summarize our main findings concerning the spin texture of the α-band. Figure 5(a) displays the spin splittings of the α-band obtained from the fits in figure 3 for the complete investigated momentum range and in (b) we draw a schematic band dispersion

based on our findings. In going away from the $\overline{\Gamma}$ point, the spin splitting increases with the in-plane momentum, in accordance with the Rashba model. In between $k_\parallel = 0.34$ and $0.5\,\text{Å}^{-1}$, the measured energy splitting is found to decrease with the in-plane momentum. Such a behavior is in sharp contrast to the Rashba model and was also observed in 1 ML Au on W(110) [56]. We conjecture that hybridization starts to develop at the inflection point, i.e. as the interaction between the α- and the adjacent β-band increases the energy splitting decreases. Finally, beyond the avoided crossing point the spin splitting recovers with a steeper slope as a consequence of the smaller effective mass, since $\Delta E \propto \alpha_{\text{RB}} \propto 1/m^\star$. Furthermore we find that the relative spin helicities of the spin-split components of the α-band are reversed upon passing the momentum region where the band bends downward. Figure 5(b) displays schematically the spin texture along the dashed line.

Figures 5(c) and (d) explain qualitatively the hybridization mechanism as revealed from the SARPES measurements. The SOC-induced hybridization between the α- and the β-band leads to a gap opening and a sign reversal in the effective mass of both bands. Close to the gap the states hybridize by mixing the orbital symmetry and the spin character of the corresponding wave functions. That way the α-band adopts the spin and orbital character of the β-band, which leads to a reversal of the sign of the momentum splitting and of the effective mass. On the other hand, beyond the hybridization gap the β-band continues to disperse with mainly p_z character (i.e. $m^\star > 0$) adopted from the α-band and approaches the adjacent γ-band, as schematically drawn in figure 5(c) for the case of no interaction between these bands. Note that in our measurements the kink in the β-band is above the Fermi level. When we turn the hybridization on (figure 5(d)), the β-band adopts the $p_{x,y}$ orbital symmetry and the spin character of the γ-band. Consequently, it disperses again hole-like and with a relative order of momentum splitting given by the γ-band which leads to a hybridization-induced reversal of the Rashba parameter. The same arguments apply for the next bands with $p_{x,y}$ symmetry, as long as other downward dispersing bands are present.

To gain a quantitative understanding of the SOC-induced hybridization we adapt an interband SOC model suggested in [22] which was successfully used to explain the gap opening in the band structure of a strongly spin-split Rashba system formed in the surface alloy BiAg$_2$. This model assumes a hybridization between two Rashba branches with opposite spin direction. In the case of Pb/Bi/Si which represents a 2DEG with weak SOC due to the Rashba effect, we introduce the opening of two hybridization gaps with the matrix elements:
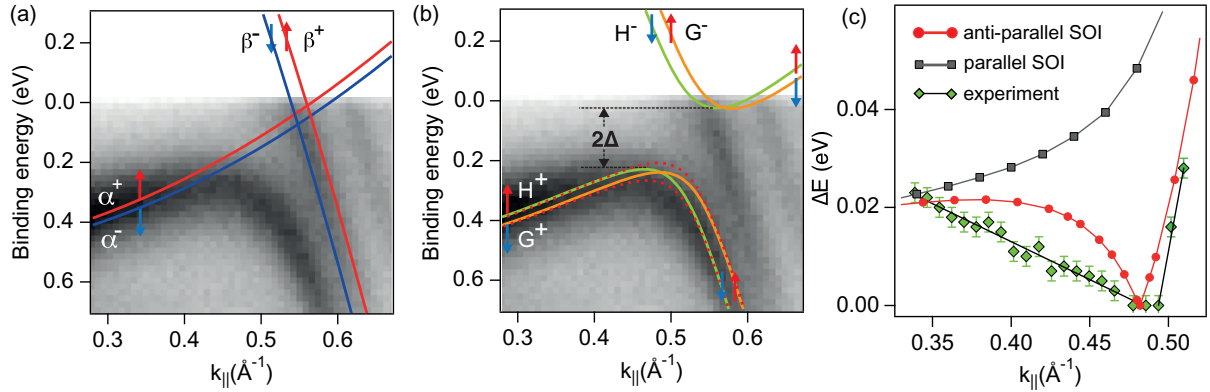
$$\Delta_1 = \langle \alpha^+ | H_{\text{HYB}} | \beta^- \rangle, \quad \Delta_2 = \langle \alpha^- | H_{\text{HYB}} | \beta^+ \rangle. \tag{3}$$

Here $|\alpha^\pm\rangle$ ($|\beta^\pm\rangle$) denotes the eigenstates of the Rashba Hamiltonian. The modified energy dispersion is calculated via [22]

$$H^\pm = \frac{1}{2}\left(\alpha^+ + \beta^-\right) \pm \sqrt{\left(\frac{\alpha^+ - \beta^-}{2}\right)^2 + \Delta_1^2}, \tag{4}$$

$$G^\pm = \frac{1}{2}\left(\alpha^- + \beta^+\right) \pm \sqrt{\left(\frac{\alpha^- - \beta^+}{2}\right)^2 + \Delta_2^2}, \tag{5}$$

where $\alpha^\pm$ and $\beta^\pm$ denote the spin-up (+) and spin-down (−) energy branches. Close to the avoided crossing point the interband SO coupling mixes the states $|\alpha^\pm\rangle$ and $|\beta^\pm\rangle$ in new

Figure 6. (a) Comparison of the band structure in the avoided crossing region with the solution of the Rashba Hamiltonian. (b) The same region as in (a) overlaid by the new solutions of the model Hamiltonian incorporating SOC due to the Rashba effect and due the interband SO coupling for an interaction of strength $\Delta_{1,2} = 120$ meV. (c) Energy splitting as a function of $k_{\parallel}$ in the hybridization region that starts at the inflection point. The measured spin splittings are compared with an interband SO coupling model that mixes states with parallel (black squares) and *anti-parallel* (red circles) spins. A closer match to the experimental findings is achieved with *anti-parallel-spin* interband SO coupling.

eigenstates:

$$|H^+\rangle = h_k|\alpha^+\rangle + \sqrt{1 - h_k^2}|\beta^-\rangle, \tag{6}$$

$$|H^-\rangle = \sqrt{1 - h_k^2}|\beta^+\rangle - h_k|\alpha^-\rangle \tag{7}$$

and

$$|G^+\rangle = g_k|\alpha^-\rangle + \sqrt{1 - g_k^2}|\beta^+\rangle, \tag{8}$$

$$|G^-\rangle = \sqrt{1 - g_k^2}|\beta^-\rangle - g_k|\alpha^+\rangle, \tag{9}$$

where h_k and g_k are k-dependent coefficients which determine the orbital and spin mixing ratio. Note that the new eigenstates are formed by a mixture of Rashba states with *anti-parallel* spins. Before we discuss the modification of the α-band dispersion induced by the interband SOC, we display in figure 6(a) the eigenvalues of the α and β bands according to the Rashba model. For the β-band we use a momentum splitting of $2k_0 = 0.021$ Å^{-1} as obtained from the vectorial spin analysis shown in figures 4(c)–(e) and an effective mass of $m^\star \approx -0.5m_e$. It is clear that this model alone can neither explain the sign reversal in the effective mass of the α-band nor the modified spin structure of the α- and the β-band across the avoided crossing point.

Figure 6(b) shows the results of applying the interband SO coupling model, in addition to the Rashba-type spin–orbit interaction, on the energy dispersion of the α-band. We find a good agreement between the experimental data and the calculated dispersion by introducing an interband SO coupling strength of $\Delta_{1,2} = 120$ meV.

In contrast to the surface alloy BiAg$_2$ investigated in [22] where the Rashba-type SOC is larger than the interband SOC ($\Delta \approx 30$ meV, $E_{RB} = \alpha_{RB}^2 m^\star/(2\hbar^2) \approx 300$ meV), the relative energy scale of SOC induced by the Rashba effect and by the interband coupling is inverted for Pb/Bi/Si. We find the interband contribution to be three orders of magnitude stronger than the Rashba contribution, $E_{RB} = 0.23$ meV. The larger Δ in Pb/Bi/Si(111) by a factor of four compared to the one found in BiAg$_2$ is understood by the fact that in Pb/Bi/Si a Rashba-split electron-like band interacts with a Rashba-split hole-like band. In BiAg$_2$ the interband SO coupling mixes electronic states which all disperse with $m^\star < 0$. The sign change of the momentum splitting for the α-band is a direct spectroscopic evidence of the mixed and k-dependent (via h_k and g_k) spin character of the corresponding new wave functions.

In the following we corroborate that in Pb/Bi/Si the interband SO coupling occurs between bands with *anti-parallel* spins (e.g. spin-flip term, $\Delta_{1,2} = \Delta^{\uparrow,\downarrow}$), instead of a coupling of bands with parallel spins (e.g. spin-conserving term, $\Delta^{\uparrow(\downarrow),\uparrow(\downarrow)}$). Although the latter scenario can also explain the modification of the α-band dispersion (see dashed lines in figure 6(b)) it fails to qualitatively reproduce the measured spin splittings as a function of momentum in the hybridization region, i.e. in the momentum region starting at the inflection point. A comparison between both models and the data is shown in figure 6(c). The model of interband SO coupling of states with parallel spins predicts neither a decrease of the spin splitting, nor a vanishing spin splitting along the band dispersion. In contrast, the model of the coupling of states with *anti-parallel* spins matches qualitatively the experimental data. That the energy splitting between the H^+ and the G^+ branch does not decrease linearly with momentum may serve as an indication that the degree of the spin polarization of the new eigenstates ($|H^+\rangle$, $|G^+\rangle$), which are formed by mixing of the Rashba spinors with opposite spin directions, is no longer 100%, although this has been assumed in the fit. Indeed, theory predicts that toward the avoided crossing point the spin polarization (P) of the states $|H^\pm\rangle$ and $|G^\pm\rangle$ as a function of $k_\parallel$ reduces according to [57, 58]

$$P(k_\parallel)^{H^\pm} = \frac{(\alpha_{k_\parallel}^+ - \beta_{k_\parallel}^-)}{\sqrt{(\alpha_{k_\parallel}^+ - \beta_{k_\parallel}^-)^2 + 4\Delta^2}}, \quad P(k_\parallel)^{G^\pm} = \frac{(\alpha_{k_\parallel}^- - \beta_{k_\parallel}^+)}{\sqrt{(\alpha_{k_\parallel}^- - \beta_{k_\parallel}^+)^2 + 4\Delta^2}}. \quad (10)$$

Consequently the measured spin polarization of the α-band toward the crossing point is reduced (i) due to the crossing of branches H^+ and G^+ and (ii) because the spin polarization of each branch is reduced due to the mixed spin character. Another indication of the action of the spin-flip term is that both bands H^+ and G^+ change their spin direction when passing the crossing point. If the spin-conserving term would dominate the spin character would not change when going along these bands [17]. Whether the action of the spin-flip, or the spin-conserving term of the SOC operator is present in a system, depends on the details of the orbital symmetry of the interacting wave functions. For example, if the β-band were p$_z$ derived then $\Delta^{\uparrow,\downarrow} = 0$ and $\Delta^{\uparrow(\downarrow),\uparrow(\downarrow)} \neq 0$, i.e. the spin-conserving part would dominate.

5. Pb/Cu(111)

In the following we substantiate that the interband SO coupling, which explains (i) the modification of the dispersion of the α-band and (ii) the sign reversal in the momentum splitting, is independent of the supporting substrate by studying QWS in Pb/Cu(111) [35, 48, 59–62]. Figure 7(a) shows the electronic structure of 8 ML Pb on Cu(111). In contrast to the electronic
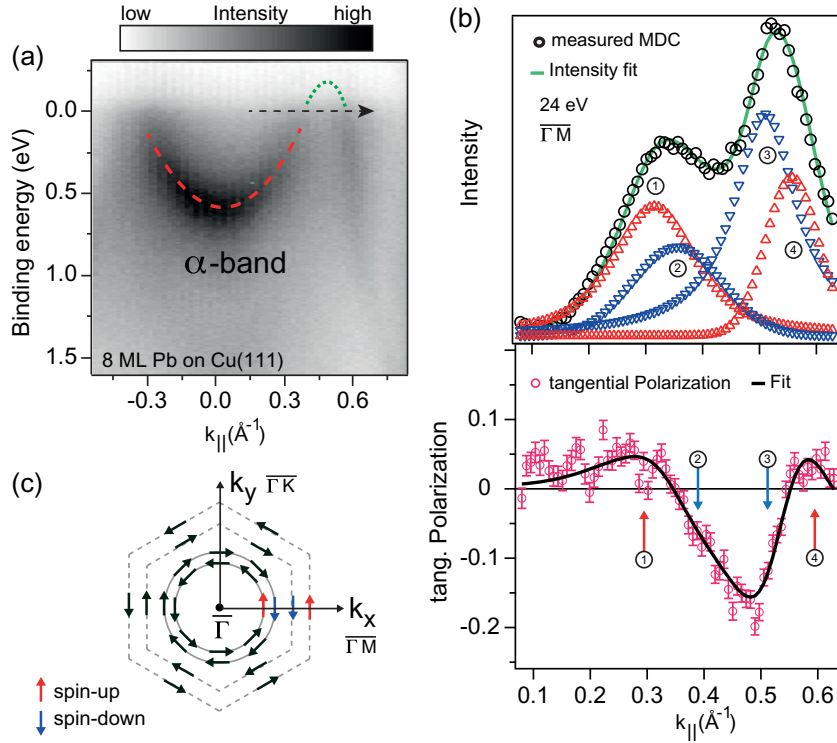
Figure 7. (a) Band structure of a 8 ML thick Pb film on Cu(111). The dashed line is a fit of the *k*-dependent intensity maxima to quantify the effective mass. The dashed arrow indicates the location of the spin-resolved measurement. (b) (upper panel) Spin-integrated momentum distribution curve and decomposition into four peaks as revealed from the two-step fitting routine and (lower panel) tangential spin polarization data and fit. (c) Spin texture of the α-band in Pb/Cu(111) at E_F.

structure of Pb/Bi/Si the effective mass of the α-band is significantly reduced from $m^\star = 3.2m_e$ to $0.86m_e$, and the pronounced change in the dispersion is situated above the Fermi level. The enhanced dispersion allows to perform a SR-MDC indicated by the dashed arrow in figure 7(a). The results and our analysis are displayed in figure 7(b) where we show the measured spin-integrated MDC close to E_F (upper panel) and the tangential spin polarization data (lower panel), respectively. We find a sign change in the momentum splitting of the α-band which is consistent with previous results obtained from Pb QWS on the Bi reconstructed Si. This is further illustrated by comparing figure 7(c), which displays the spin alignment at E_F, with the inset of figure 5(b).

6. Conclusions

To summarize, we have identified a momentum region in Pb QWS where the description of the Rashba effect breaks down due to the interband SOC. Essential is that this coupling leads to a hybridization of Rashba states with *anti-parallel* spins thereby causing the pronounced change in the dispersion of the α-band, a sign change of the momentum splitting, and in particular a

vanishing spin splitting toward the avoided crossing point. These modifications clearly reflect the SOC-induced hybridization mechanism because of the mixed spin and orbital character of the new wave functions. This finding is consistent with the results obtained from QWS in Pb on Cu(111). Furthermore, we have found that the interband contribution in Pb/Bi/Si is three orders of magnitude stronger than the SOI contribution by the Rashba effect. It is expected that this ratio is smaller in Pb/Pb/Si and larger in Pb/Ag/Si due to the different effective masses of the α-band.

Acknowledgments

References

[1] Dil J H 2009 Spin and angle resolved photoemission on non-magnetic low-dimensional systems *J. Phys.: Condens. Matter* **21** 403001

[2] Ishizaka K *et al* 2011 Giant Rashba-type spin splitting in bulk BiTeI *Nature Mater.* **10** 521

[3] Landolt G *et al* 2012 Disentanglement of surface and bulk Rashba spin splittings in noncentrosymmetric BiTeI *Phys. Rev. Lett.* **109** 116403

[4] Ast C R, Henk J, Ernst A, Moreschini L, Falub M C, Pacilé D, Bruno P, Kern K and Grioni M 2007 Giant spin splitting through surface alloying *Phys. Rev. Lett.* **98** 186807

[5] Yaji K *et al* 2010 Large Rashba spin splitting of a metallic surface-state band on a semiconductor surface *Nature Commun.* **1** 17

[6] Höpfner P *et al* 2012 Three-dimensional spin rotations at the fermi surface of a strongly spin–orbit coupled surface system *Phys. Rev. Lett.* **108** 186801

[7] Wells J W *et al* 2009 Nondegenerate metallic states on Bi(114): a one-dimensional topological metal *Phys. Rev. Lett.* **102** 096802

[8] Okuda T *et al* 2010 Large out-of-plane spin polarization in a spin-splitting one-dimensional metallic surface state on Si(557)–Au *Phys. Rev.* B **82** 161410

[9] Tegenkamp C, Lükermann D, Pfnür H, Slomski B, Landolt G and Dil J H 2012 Fermi nesting between atomic wires with strong spin–orbit coupling *Phys. Rev. Lett.* **109** 266401

[10] Hasan M Z and Kane C L 2010 Colloquium: topological insulators *Rev. Mod. Phys.* **82** 3045

[11] Hsieh D *et al* 2009 Observation of unconventional quantum spin textures in topological insulators *Science* **323** 919

[12] Hsieh D *et al* 2009 A tuneable topological insulator in the spin helical dirac transport regime *Nature* **460** 1101

[13] Xu S Y *et al* 2011 Topological phase transition and texture inversion in a tunable topological insulator *Science* **332** 560

[14] Souma S, Kosaka K, Sato T, Komatsu M, Takayama A, Takahashi T, Kriener M, Segawa K and Ando Y 2011 Direct measurement of the out-of-plane spin texture in the Dirac-cone surface state of a topological insulator *Phys. Rev. Lett.* **106** 216803

[15] Eremeev S V *et al* 2012 Atom-specific spin mapping and buried topological states in a homologous series of topological insulators *Nature Commun.* **3** 635

[16] Cao Y *et al* 2012 Coupled spin–orbital texture in a prototypical topological insulator arXiv:1211.5998

[17] Ebert H, Freyer H and Deng M 1997 Manipulation of the spin–orbit coupling using the dirac equation for spin-dependent potentials *Phys. Rev.* B **56** 9454

[18] Rybkin A G, Shikin A M, Marchenko D, Varykhalov A and Rader O 2012 Spin-dependent avoided-crossing effect on quantum-well states in Al/W(110) *Phys. Rev.* B **85** 045425

[19] He K *et al* 2010 Direct spectroscopic evidence of spin-dependent hybridization between Rashba-split surface states and quantum-well states *Phys. Rev. Lett.* **104** 156805

[20] Frantzeskakis E, Pons S, Mirhosseini H, Henk J, Ast C R and Grioni M 2008 Tunable spin gaps in a quantum-confined geometry *Phys. Rev. Lett.* **101** 196805

[21] Mirhosseini H, Henk J, Ernst A, Ostanin S, Chiang C-T, Yu P, Winkelmann A and Kirschner J 2009 Unconventional spin topology in surface alloys with Rashba-type spin splitting *Phys. Rev.* B **79** 245428

[22] Bentmann H, Abdelouahed S, Mulazzi M, Henk J and Reinert F 2012 Direct observation of interband spin–orbit coupling in a two-dimensional electron system *Phys. Rev. Lett.* **108** 196801

[23] Guo Y *et al* 2004 Superconductivity modulated by quantum size effects *Science* **306** 1915

[24] Brun C, Hong I-P, Patthey F, Sklyadneva I Y, Heid R, Echenique P M, Bohnen K P, Chulkov E V and Schneider W-D 2009 Reduction of the superconducting gap of ultrathin Pb islands grown on Si(111) *Phys. Rev. Lett.* **102** 207002

[25] Eom D, Qin S, Chou M-Y and Shih C K 2006 Persistent superconductivity in ultrathin Pb films: a scanning tunneling spectroscopy study *Phys. Rev. Lett.* **96** 027005

[26] Budde K, Abram E, Yeh V and Tringides M C 2000 Uniform, self-organized, seven-step height Pb/Si(111) − (7×7) islands at low temperatures *Phys. Rev.* B **61** R10602

[27] Kirchmann P S, Rettig L, Zubizarreta X, Silkin V M, Chulkov E V and Bovensiepen U 2010 Quasiparticle lifetimes in metallic quantum-well nanostructures *Nature Phys.* **6** 782

[28] Heslinga D R, Weitering H H, van der Werf D P, Klapwijk T M and Hibma T 1990 Atomic-structure-dependent Schottky barrier at epitaxial Pb/Si(111) interfaces *Phys. Rev. Lett.* **64** 1589

[29] Ricci D A, Miller T and Chiang T C 2004 Chemical tuning of metal–semiconductor interfaces *Phys. Rev. Lett.* **93** 136801

[30] Slomski B, Meier F, Osterwalder J and Dil J H 2011 Controlling the effective mass of quantum well states in Pb/Si(111) by interface engineering *Phys. Rev.* B **83** 035409

[31] Dil J H, Meier F, Lobo-Checa J, Patthey L, Bihlmayer G and Osterwalder J 2008 Rashba-type spin–orbit splitting of quantum well states in ultrathin Pb films *Phys. Rev. Lett.* **101** 266802

[32] Slomski B, Landolt G, Meier F, Patthey L, Bihlmayer G, Osterwalder J and Dil J H 2011 Manipulating the Rashba-type spin splitting and spin texture of Pb quantum well states *Phys. Rev.* B **84** 193406

[33] Meier F, Dil J H and Osterwalder J 2009 Measuring spin polarization vectors in angle-resolved photoemission spectroscopy *New J. Phys.* **11** 125008

[34] Hoesch M, Greber T, Petrov V N, Muntwiler M, Hengsberger M, Auwaerter W and Osterwalder J 2002 Spin-polarized fermi surface mapping *J. Electron Spectrosc. Relat. Phenom.* **124** 263

[35] Dil J H, Kim J W, Gokhale S, Tallarida M and Horn K 2004 Self-organization of Pb thin films on Cu(111) induced by quantum size effects *Phys. Rev.* B **70** 045405

[36] Takayanagi K, Kolb D M, Kambe K and Lehmpfuhl G 1980 Deposition of monolayer and bulk lead on Ag(111) studied in vacuum and in an electrochemical cell *Surf. Sci.* **100** 407

[37] Wan K J, Guo T, Ford W K and Hermanson J C 1991 Initial growth of Bi films on a Si(111) substrate: two phases of $\sqrt{3} \times \sqrt{3}$ low-energy-electron-diffraction pattern and their geometric structures *Phys. Rev.* B **44** 3471

[38] Nitta J, Akazaki T, Takayanagi H and Enoki T 1997 Gate control of spin–orbit interaction in an inverted $In_{0.53}Ga_{0.47}As/In_{0.52}Al_{0.48}As$ heterostructure *Phys. Rev. Lett.* **78** 1335

[39] LaShell S, McDougall B A and Jensen E 1996 Spin splitting of an Au(111) surface state band observed with angle resolved photoelectron spectroscopy *Phys. Rev. Lett.* **77** 3419

[40] Nicolay G, Reinert F, Hüfner S and Blaha P 2001 Spin–orbit splitting of the L-gap surface state on Au(111) and Ag(111) *Phys. Rev.* B **65** 033407

[41] Hoesch M, Muntwiler M, Petrov V N, Hengsberger M, Patthey L, Shi M, Falub M, Greber T and Osterwalder J 2004 Spin structure of the Shockley surface state on Au(111) *Phys. Rev.* B **69** 241401

[42] Tamai A, Meevasana W, King P D C, Nicholson C W, de la Torre A, Rozbicki E and Baumberger F 2013 Spin–orbit splitting of the Shockley surface state on Cu(111) *Phys. Rev.* B **87** 075113

[43] Ast C R, Wittich G, Wahl P, Vogelgesang R, Pacilé D, Falub M C, Moreschini L, Papagno M, Grioni M and Kern K 2007 Local detection of spin–orbit splitting by scanning tunneling spectroscopy *Phys. Rev.* B **75** 201401

[44] Meier F, Dil J H, Lobo-Checa J, Patthey J and Osterwalder J 2008 Quantitative vectorial spin analysis in angle-resolved photoemission: Bi/Ag(111) and Pb/Ag(111) *Phys. Rev.* B **77** 165431

[45] Ast C R *et al* 2008 Spin–orbit split two-dimensional electron gas with tunable Rashba and Fermi energy *Phys. Rev.* B **77** 081407

[46] Meier F, Petrov V, Guerrero S, Mudry C, Patthey L, Osterwalder J and Dil J H 2009 Unconventional Fermi surface spin textures in the Bi_xPb_{1-x}/Ag(111) surface alloy *Phys. Rev.* B **79** 241408

[47] Gierz I, Suzuki T, Frantzeskakis E, Pons S, Ostanin S, Ernst A, Henk J, Grioni M, Kern K and Ast C R 2009 Silicon surface with giant spin splitting *Phys. Rev. Lett.* **103** 046803

[48] Mathias S *et al* 2010 Quantum-well-induced giant spin–orbit splitting *Phys. Rev. Lett.* **104** 066802

[49] Heinzmann U and Dil J H 2012 Spin–orbit induced photoelectron spin polarization in angle-resolved photoemission from both atomic and condensed matter targets *J. Phys.: Condens. Matter* **24** 173001

[50] Schwarz K and Blaha P 2003 Solid state calculations using Wien2k *Comput. Mater. Sci.* **28** 259

[51] Slomski B, Landolt G, Bihlmayer G, Osterwalder J and Dil J H 2013 Tuning the Rashba effect in Pb quantum well states via a variable Schottky barrier *Sci. Rep.* **3** 1963

[52] Horn K, Reihl B, Zartner A, Eastman D E, Hermann K and Noffke J 1984 Electronic energy bands of lead: angle-resolved photoemission and band-structure calculations *Phys. Rev.* B **30** 1711

[53] Upton M H, Miller T and Chiang T C 2005 Unusual band dispersion in Pb films on Si(111) *Phys. Rev.* B **71** 033403

[54] Dil J H, Kampen T U, Hülsen B, Seyller T and Horn K 2007 Quantum size effects in quasi-free-standing Pb layers *Phys. Rev.* B **75** 161401

[55] Rybkin A G, Krasowskii E E, Marchenko D, Chulkov E V, Rader O and Shikin A M 2012 Topology of spin polarization of the 5d states on W(110) and Al/W(110) surfaces *Phys. Rev.* B **86** 035117

[56] Varykhalov A, Sánchez-Barriga J, Shikin A M, Gudat W, Eberhardt W and Rader O 2008 Quantum cavity for spin due to spin–orbit interaction at a metal boundary *Phys. Rev. Lett.* **101** 256601

[57] Fabian J and Sarma S D 1998 Spin relaxation of conduction electrons in polyvalent metals: theory and a realistic calculation *Phys. Rev. Lett.* **81** 5624

[58] Gradhand M, Czerner M, Fedorov D M, Zahn P, Yavorsky B Y, Szunyogh L and Mertig I 2009 Spin polarization on fermi surfaces of metals by the KKR method *Phys. Rev.* B **80** 224413

[59] Braun J, Ruggerone P, Zhang G, Toennies J P and Benedek G 2009 Surface phonon dispersion curves of thin Pb films on Cu(111) *Phys. Rev.* B **79** 205423

[60] Zugarramurdi A, Zabala N, Silkin V M, Borisov A G and Chulkov E V 2009 Lifetimes of quantum well states and resonances in Pb overlayers on Cu(111) *Phys. Rev.* B **80** 115425

[61] Zugarramurdi A, Zabala N, Silkin V M, Chulkov E V and Borisov A G 2012 Quantum-well states with image state character for Pb overlayers on Cu(111) *Phys. Rev.* B **86** 075434

[62] Otero R, Vázquez de Parga A L and Miranda R 2002 Observation of preferred heights in Pb nanoislands: a quantum size effect *Phys. Rev.* B **66** 115401